Rotational dynamics of proteins from spin relaxation times and molecular dynamics simulations

O. H. Samuli Ollila,*,†,‡ Harri A. Heikkinen,† and Hideo Iwaï†

†*Insititute of Biotechnology, University of Helsinki*

‡*Institute of Organic Chemistry and Biochemistry, Czech Academy of Sciences, Prague 6, Czech Republic*

E-mail: samuli.ollila@helsinki.fi

Abstract

Conformational fluctuations and rotational tumbling of proteins can be experimentally accessed with nuclear spin relaxation experiments. However, interpretation of molecular dynamics from the experimental data is often complicated, especially for molecules with anisotropic shape. Here we apply classical molecular dynamics simulations to interpret the conformational fluctuations and rotational tumbling of proteins with arbitrarily anisotropic shape. The direct calculation of spin relaxation times from simulation data did not reproduce the experimental data. This was successfully corrected by scaling the overall rotational diffusion coefficients around the protein inertia axes with a constant factor. The achieved good agreement with experiments allowed the interpretation of the internal and overall dynamics of proteins with significantly anisotropic shape. The overall rotational diffusion was found to be brownian, having only a short subdiffusive region below 0.12 ns. The presented methodology can be applied to interpret rotational dynamics and conformation fluctuations of proteins with arbitrary anisotropic shape. However, a water model with more realistic dynamical properties is probably required for intrinsically disordered proteins.

Introduction

Conformational fluctuations and the entropy of proteins play a significant role in their functionality and interactions with other biomolecules. Conformational fluctuations and the overall brownian tumbling of proteins are experimentally accessible through the spin relaxation times of ^{15}N and ^{13}C nuclei measured with nuclear magnetic resonance (NMR) techniques.[1–7] The spin relaxation rates have been used to, for example, analyze conformational entropies,[1,8–10] binding entropies,[1,11] resolve sampled structures[3–5,12] and validate molecular dynamics simulations.[13–17] These analyzes are almost exclusively based on the separation of the internal conformational fluctuations and the overall rotational tumbling.[18,19] Also the isotropic overall diffusion is often assumed, while analysis of anisotropic molecules is sig-

nificantly more complicated.[1,2,20–23] Thus, the new approaches are needed to interpret spin relaxation times measured from anisotropic or intrinsically disordered molecules.

Classical molecular dynamics (MD) simulation methods are promising tools to interpret spin relaxation experiments for molecules with significantly anisotropic shape or correlations between internal and overall rotational motions. Practical applications are, however, limited by inaccuracies in the force field descriptions and the available time scales in the simulations.[16,17,24–26] The main issues have been the overestimated overall rotational diffusion of proteins due to inaccuracies in water models[25] and the insufficient accuracy of correlation functions calculated from single molecules in MD simulations.[26,27]

In this work we overcome these issues by assuming that the overall rotational dynamics of protein follows anisotropic rigid body diffusion. Diffusion coefficients around inertia axes are directly calculated from angular displacements. The diffusion coefficients are then used to determine the contribution of the overall rotational tumbling to the rotational correlation functions of N-H bonds. This reduces the required simulation length for the accurate determination of the rotational correlation functions. Furthermore, the overestimated overall brownian tumbling rates due to the inaccurate water model can be corrected during the correlation function calculation by scaling the diffusion coefficients in all directions with a constant factor. The corrected correlation functions can be used to interpret the spin relaxation experiments for proteins with arbitrarily anisotropic shapes.

The developed approach is demonstrated by interpreting the experimental spin relaxation data of C-terminal domains of TonB proteins from *Helicobacter pyroli* (*Hp*TonB-92)[28] and from *Pseudomonas aeruginosa* (*Pa*TonB-96),[29] having 92 and 96 residues, respectively. Both proteins have significantly anisotropic shape, which would complicate the standard spin relaxation data analysis.[1,2,20–23]

Methods

Spin relaxation experiments and rotational dynamics of molecules

Molecular dynamics of the protein backbone residues and spin relaxation experiments can be connected by using the spectral density $J(\omega)$

$$J(\omega) = 2\int_0^\infty C(t)\cos(\omega t)\mathrm{d}t, \tag{1}$$

which is the Fourier transformation of the second order rotational correlation function for N-H bond vector

$$C(t) = \langle \frac{3}{2}\cos^2\theta_{t'+t} - \frac{1}{2}\rangle_{t'}, \tag{2}$$

where $\theta_{t'+t}$ is the N-H bond angle between times t' and $t'+t$ and angular brackets refer to the ensemble average. Connection to the experimentally measured spin relaxation times T_1, T_2 and the NOE relaxation are given by the Redfield equations[30,31]

$$\begin{aligned}\frac{1}{T_1} =& \frac{d_{\mathrm{NH}}^2 N_{\mathrm{H}}}{20}\Big[J(\omega_{\mathrm{H}}-\omega_{\mathrm{N}}) + 3J(\omega_{\mathrm{N}}) + 6J(\omega_{\mathrm{N}}+\omega_{\mathrm{H}})\Big] \\ &+ \frac{(\sigma\omega_{\mathrm{N}})^2}{15}J(\omega_{\mathrm{N}}),\end{aligned} \tag{3}$$

$$\begin{aligned}\frac{1}{T_2} =& \frac{1}{2}\frac{d_{\mathrm{NH}}^2 N_{\mathrm{H}}}{20}\Big[4J(0) + 3J(\omega_{\mathrm{N}}) + J(\omega_{\mathrm{H}}-\omega_{\mathrm{N}}) + 6J(\omega_{\mathrm{H}}) \\ &+ 6J(\omega_{\mathrm{N}}+\omega_{\mathrm{H}})\Big] + \frac{(\sigma\omega_{\mathrm{N}})^2}{90}[4J(0) + 3J(\omega_{\mathrm{N}})],\end{aligned} \tag{4}$$

$$\mathrm{NOE} = 1 + \frac{d_{\mathrm{NH}}^2 N_{\mathrm{H}}}{20}\Big[6J(\omega_{\mathrm{N}}+\omega_{\mathrm{H}}) + J(\omega_{\mathrm{H}}-\omega_{\mathrm{N}}))\Big]\frac{\gamma_{\mathrm{H}}T_1}{\gamma_{\mathrm{N}}}, \tag{5}$$

where ω_{N} and ω_{H} are the Larmor angular frequencies of ^{15}N and ^{1}H respectively, and the number of bound protons $N_{\mathrm{H}} = 1$ for N-H bonds. The dipolar coupling constant is given by

$$d_{\mathrm{NH}} = -\frac{\mu_0\hbar\gamma_{\mathrm{H}}\gamma_{\mathrm{N}}}{4\pi\langle r_{\mathrm{NH}}^3\rangle},$$

where μ_0 is the magnetic constant or vacuum permeability, $\hbar$ is the reduced Planck constant, γ_{N} and γ_{H} are the gyromagnetic constants of ^{15}N and ^{1}H, respectively. The average cubic length is calculated as $\langle r_{\mathrm{NH}}^3 \rangle = (0.101 \text{ nm})^3$ and the value of $\Delta\sigma = -160$ ppm is used for the chemical shift anisotropy of N-H bonds in proteins.[31,32]

Spin relaxation experiments are typically interpreted for proteins by assuming that the motions related to the overall brownian tumbling and conformational fluctuations are independent. The rotational correlation function for each N-H bond can be then written as[1,2,18,19,33]

$$C(t) = C_I(t) C_O(t), \tag{6}$$

where $C_I(t)$ and $C_O(t)$ are correlation functions for the internal and overall rotations, respectively. Conformational fluctuations can be described in this approximation by using the square of the order parameter respect to molecular axes S^2, which is given by the plateau of the internal rotational correlation function. Timescales for the fluctuations can be characterized by using the effective correlation time

$$\tau_{\mathrm{eff}} = \int_0^\infty C_I'(t) \mathrm{d}t, \tag{7}$$

where $C_I'(t) = \frac{C_I - S^2}{1 - S^2}$ is the reduced correlation function.[19]

The overall rotational correlation function is often described by approximating the protein as a rigid body. For arbitrarily anisotropic molecules, the correlation functions can be presented as a sum of five exponentials[2,20]

$$C_O(t) = \sum_{j=1}^{5} A_j e^{-t/\tau_j}, \tag{8}$$

where the prefactors A_j depend on the directions of chemical bonds respect to the molecular axes[20,22] and the time constants τ_j are related to the diffusion constants around three

principal axes of a molecule (D_x, D_y, and D_z) through equations[2,20]

$$\begin{aligned}
\tau_1 &= (4D_x + D_y + D_z)^{-1} \\
\tau_2 &= (D_x + 4D_y + D_z)^{-1} \\
\tau_3 &= (D_x + D_y + 4D_z)^{-1} \\
\tau_4 &= [6(D_{\mathrm{av}} + (D_{\mathrm{av}}^2 - L^2)^{-1/2}]^{-1} \\
\tau_5 &= [6(D_{\mathrm{av}} - (D_{\mathrm{av}}^2 - L^2)^{-1/2}]^{-1},
\end{aligned} \tag{9}$$

where $D_{\mathrm{av}} = \frac{1}{3}(D_x + D_y + D_z)$ and $L^2 = \frac{1}{3}(D_xD_y + D_xD_z + D_yD_z)$.

The simplest approach to extract molecular dynamics from the experimental data is the original "model-free analysis",[19] where an isotropic diffusion is assumed for the overall rotation of the protein. This reduces Eq. 8 to a monoexponential form and the overall rotational dynamics can be described with a single time constant τ_c. Also the internal correlation functions for each residue are assumed to decay exponentially with a single time constant τ_{eff} toward to the square of the order parameter S^2. The three parameters (τ_c, τ_{eff}, and S^2) can be then successfully resolved from a fit to the experimental data. However, the number of parameters to be fitted increases if the protein experiences an anisotropic overall diffusion or has several timescales for internal motions. In this case the fitting becomes often ambiguous, even if the experimental data would be measured with multiple magnetic field strengths.[1,22,34] The anisotropic rotational diffusion is sometimes described with hydrodynamical calculations, but they are sensitive to the estimation of the hydration shell around the protein.[35]

Rough estimate for the timescale of overall rotational dynamics is often given by using the T_1/T_2 ratio.[31] This is based on the assumptions that T_1 and T_2 are independent of the internal motions and that the overall dynamics is isotropic. The spectral density then reduces to

$$J'(\omega) = S^2 \frac{\tau_c'}{1 + (\omega\tau_c')^2} \tag{10}$$

and the correlation time describing the overall rotational motion, τ_c', can be estimated by numerically minimizing the equation

$$\frac{T_1}{T_2} \approx \frac{\frac{1}{2}\frac{d_{\mathrm{NH}}^2 N_{\mathrm{H}}}{20}\left[4J'(0)+3J'(\omega_{\mathrm{N}})+J'(\omega_{\mathrm{H}}-\omega_{\mathrm{N}})+6J'(\omega_{\mathrm{H}})+6J'(\omega_{\mathrm{N}}+\omega_{\mathrm{H}})\right]+\frac{(\sigma\omega_{\mathrm{N}})^2}{90}[4J'(0)+3J'(\omega_{\mathrm{N}})]}{\frac{d_{\mathrm{NH}}^2 N_{\mathrm{H}}}{20}\left[J'(\omega_{\mathrm{H}}-\omega_{\mathrm{N}})+3J'(\omega_{\mathrm{N}})+6J'(\omega_{\mathrm{N}}+\omega_{\mathrm{H}})\right]+\frac{(\sigma\omega_{\mathrm{N}})^2}{15}J'(\omega_{\mathrm{N}})} \tag{11}$$

with respect to the experimentally measured T_1/T_2 ratio.

Rotational dynamics from molecular dynamics simulations

A classical molecular dynamics simulation gives a trajectory for each atom in the system as a function of time. Rotational correlation functions for each bond can be then directly calculated from the trajectories by Eq. 2 and used to calculate the spin relaxation times through Eqs. 1-5. The resulting values can be compared to experimental data in order to assess simulation model quality[13–17,36] or to interpret experiments.[36]

The direct comparison with experiments is, however, often complicated by the insufficient statistics for the calculated correlation functions and the overestimated rotational diffusion due to inaccuracies in water models.[25,26] Here we show that the statistical accuracy of the contribution of the overall tumbling to the correlation functions, $C_0(t)$ in Eq. 6, can be increased for rigid proteins by directly calculating the diffusion coefficients of the inertia axes. The rotational diffusion coefficients can be related to the timescales τ_j of the correlation function for anisotropic rigid body rotation in Eq. 8 by using the relations in Eq. 9.[20]

The rotational diffusion coefficients are calculated by fitting a linear slope to the square angle deviation of the inertia axes (see below). This requires less simulation data for the good statistics than a direct fit of the multiexponential sum in Eq. 8 to the rotational correlation function calculated from MD simulation. In addition, the overestimated rotational diffusion due to water model[25] can be corrected by scaling the diffusion coefficients around all inertia axes by a constant factor. This approach takes into account the anisotropic shape of the

molecule. This is a significant advancement to the previous studies, which assume isotropic rotational diffusion with a single exponential rotational correlation function[10,14–16,37] or use order parameters to compare simulations with experimental data.[13,16,17,37]

The practical analysis can be divided into seven steps:

1) The total rotational correlation functions $C(t)$ for N-H bond vectors in a protein are directly calculated from MD simulation trajectory by applying Eq. 2.

2) The rotational correlation functions for internal dynamics $C_I(t)$ are calculated from MD simulation trajectory by removing overall rotation of the protein.

3) The overall and internal motions are assumed to be independent and the overall rotational correlation function is calculated from Eq. 6 as $C_O(t) = C(t)/C_I(t)$.

4) The mean square angle deviations of rotation around protein inertia axes are calculated from MD simulation trajectory.

5) Rotational diffusion constants D_x, D_y, and D_z around inertia axes are calculated by fitting a straight line to the mean square angle deviations

$$\begin{aligned} \langle \Delta\alpha^2_{t'+t} \rangle_{t'} &= 2D_x t \\ \langle \Delta\beta^2_{t'+t} \rangle_{t'} &= 2D_y t \\ \langle \Delta\gamma^2_{t'+t} \rangle_{t'} &= 2D_z t, \end{aligned} \tag{12}$$

where $\langle \Delta\alpha^2_{t'+t} \rangle_{t'}$, $\langle \Delta\beta^2_{t'+t} \rangle_{t'}$, and $\langle \Delta\gamma^2_{t'+t} \rangle_{t'}$ are the mean square angle deviations from the shortest protein inertia axis to the longest, respectively.

6) Contribution of the overall rotational tumbling to all correlation functions is assumed to follow Eq. 8 with the timescales τ_j calculated from the rotational diffusion constants by using the relations in Eq. 9. Weighting factors A_j are determined by fitting the equation to the overall rotational correlation functions calculated from MD simulations in step 3.

7) The new correlation functions are calculated by substituting internal correlation functions, $C_I(t)$, from step 2 and anisotropic rigid body rotational correlation functions, $C_O(t)$, from

step 6 to Eq. 6 giving

$$C_N(t) = C_I(t) \sum_{j=1}^{5} A_j e^{-t/\tau_j}. \quad (13)$$

These correlation functions are then used to calculate spin relaxation times from Eqs. 1-5. The incorrect overall rotational diffusion due to a water model can be corrected at this point by scaling the rotational diffusion coefficients, i.e. timescales τ_j, with a constant factor before calculating new correlation functions from Eq. 13.

Simulation and analysis details

All simulations were performed using Gromacs 5[46] and Amber ff99SB- ILDN[47] force field for proteins. The protein was solvated to tip3p,[48] tip4p,[48] or OPC4[49] water models. Initial structures were taken from NMR structures of *Hp*TonB-92 (PDB code: 5LW8)[28] and *Pa*TonB-96 (PDB code: 6FIP).[29] The temperature was coupled to the desired value with the v-rescale thermostat[50] and the pressure was isotropically set to 1 bar using Parrinello-Rahman barostat.[51] Timestep was 2 fs, Lennart-Jones interactions were cut-off at 1.0 nm, PME[52,53] was used for electrostatics and LINCS was used to constraint all bond lengths.[54] The simulated systems are listed in Table 1 with the references giving access to the trajectories and the related simulation files.

The rotational correlation functions are calculated with *gmx rotacf* from Gromacs package.[55] The overall rotation was removed for $C_I(t)$ calculation by using a fit option of the *gmx trjconv* tool in Gromacs package.[55] The order parameters S^2 were determined by averaging rotational correlation functions from oriented trajectory, $C_I(t)$, over the lag times above 50 ns. The effective correlation times were then calculated by Eq. 7. Inertia axes of proteins were calculated with *compute_inertia_tensor* function from MDTraj python library.[56]

Spectral density was calculated by fitting a sum of 471 exponentials with timescales from

Table 1: Simulated systems and rotational diffusion coefficients ($rad^2 \cdot 10^7/s$) calculated from simulations.

Protein	Water[a]	T (K)[b]	t_s(ns)[c]	t_a(ns)[d]	D_x	D_y	D_z	$D_{\|\|}/D_\perp$[e]	D_{av}[f]	files
*Pa*TonB-96	tip4p	298	400	390	1.81 ± 0.01	2.06 ± 0.03	4.55 ± 0.03	2.35 ± 0.04	2.80 ± 0.02	[38]
*Pa*TonB-96	tip4p	310	400	390	2.60 ± 0.02	2.22 ± 0.05	5.0 ± 0.1	2.07 ± 0.09	3.26 ± 0.07	[39]
*Pa*TonB-96	OPC4	310	1200	1190	2.01 ± 0.01	2.19 ± 0.01	5.01 ± 0.03	2.39 ± 0.02	3.07 ± 0.01	[40]
*Hp*TonB-92	tip3p	310	570	370	8.25 ± 0.05	7.67 ± 0.06	15.9 ± 0.3	1.99 ± 0.06	10.6 ± 0.2	[41]
*Hp*TonB-92	tip3p	303	800	790	6.24 ± 0.02	7.04 ± 0.03	11.9 ± 0.2	1.80 ± 0.03	8.40 ± 0.07	[42]
*Hp*TonB-92	tip4p	310	470	370	3.6 ± 0.1	3.24 ± 0.01	6.3 ± 0.3	1.8 ± 0.1	4.4 ± 0.2	[43]
*Hp*TonB-92	tip4p	303	400	200	2.7 ± 0.1	2.71 ± 0.02	5.6 ± 0.5	2.1 ± 0.2	3.7 ± 0.2	[44]
*Hp*TonB-92	OPC4	310	800	790	2.85 ± 0.01	2.70 ± 0.01	5.56 ± 0.01	2.00 ± 0.01	3.70 ± 0.01	[45]

[a] Water model used in simulation.
[b] Simulation temperature
[c] Total simulation time
[d] Analyzed simulation time
[e] $D_{||} = D_z$, $D_\perp = \frac{1}{2}(D_x + D_y)$
[f] $D_{av} = \frac{1}{3}(D_x + D_y + D_z)$

1 ps to 50 ns with logarithmic spacing

$$C_N(t) = \sum_{i=1}^{N} \alpha_i e^{-t/\tau_i} \tag{14}$$

to the new correlation function from Eq. 13 by using the *lsqnonneg* routine in MATLAB.[57] The Fourier transform was then calculated by using the analytical function for the sum of exponentials

$$J(\omega) = 2\sum_{i=1}^{N} \alpha_i \frac{\tau_i}{1+\omega^2\tau_i^2}. \tag{15}$$

A similar approach has been previously used for the lamellar lipid and surfactant systems in combination with solid state NMR experiments.[58,59] All the computer programs used for the analysis are available at.[60]

Spin relaxation experiments

NMR experiments were recorded on a Bruker Avance III 850 NMR spectrometer equipped with cryogenic probe head. The longitudinal (T_1), transverse (T_2), and ^{1}H-^{15}N-heteronuclear NOE spin relaxation times for the backbone ^{15}N atoms of *Hp*TonB-92[28] were collected at 303 K using the well-established NMR pulse sequences described previously.[31,61] The similarly detected spin relaxation data for *Pa*TonB-96 at 298 K is reported in a another publication.[29] The T_1 and T_2 relaxation times were measured using the following delay times: 10, 50, 100, 200, 300, 500, 800, 1000, 1200 and 2000 ms, and 16, 64, 96, 128, 156, 196, 224 and 256 ms for CPMG pulse train with 1.0 ms interval for T_2 relaxation times, respectively. The relaxation rates ($R_1 = 1/T_1$, $R_2 = 1/T_2$) were calculated as an exponential fit of a single exponential decay to peak intensity values: $I(t) = I_0 \exp(-t/T_1)$, or $I(t) = I_0 \exp(-t/T_2)$, where $I(t)$ is the peak volume at a time t. The ^{15}N{^{1}H}-NOE measurements were carried out with a relaxation delay of 5 s with and without saturation of the amide protons. The ^{15}N{^{1}H}-NOE values were derived from the volumes of the HSQC peaks using the equation of $\nu = I/I_0$. The relaxation data was processed and analyzed using Bruker Dynamic Center

software (version 2.1.8).

Results and Discussion

Global rotational dynamics of protein

The mean square angle deviations for the rotation of *Pa*TonB-96 protein construct around inertia axes in the simulation with OPC4 water model are shown in Fig. 1. This is the longest simulation data set in this work (1.2 μs) and the linear behavior of the mean square angle deviations are observed for the lag times up to one hundredth of the total simulation length (12 ns), which is expected to be the maximum lag time for the good statistics of rotational dynamics analyzed from a single molecule in MD simulations.[27] Deviations from the linear behavior are only seen with the lag times longer than this limit, as also demonstrated for the shorter simulations in Figs. S1 and S2 in Supplementary Information with tip4p water at two different temperatures. The plots with log-log scale in Figs. 1, S1 and S2 reveal a weakly subdiffusive region only below very short timescales of approximately 0.12 ns. Thus, we conclude that the protein experiences the brownian rotational tumbling with a good approximation. The diffusion coefficients can be then calculated from the slope of the mean square angle deviations according to Eq. 12 by using the lag times less than one hundredth of the total MD simulation length. The error bars were calculated varying the lag time with 1 ns to both directions. The data from *Hp*TonB-92 protein (not shown) led to similar conclusions.

The resulting rotational diffusion constants from different simulations are summarized in Table 1. As expected, the rotational diffusion coefficients increase with the temperature and the decreasing size of a protein. The values are, however, larger than expected from the experimental T_1/T_2 ratio analyzed with Eq. 11 and from the previously reported values for proteins with similar sizes,[62] especially when tip3p water model is used. Similar results were previously explained by the overestimated water self-diffusion of tip3p water model.[25]

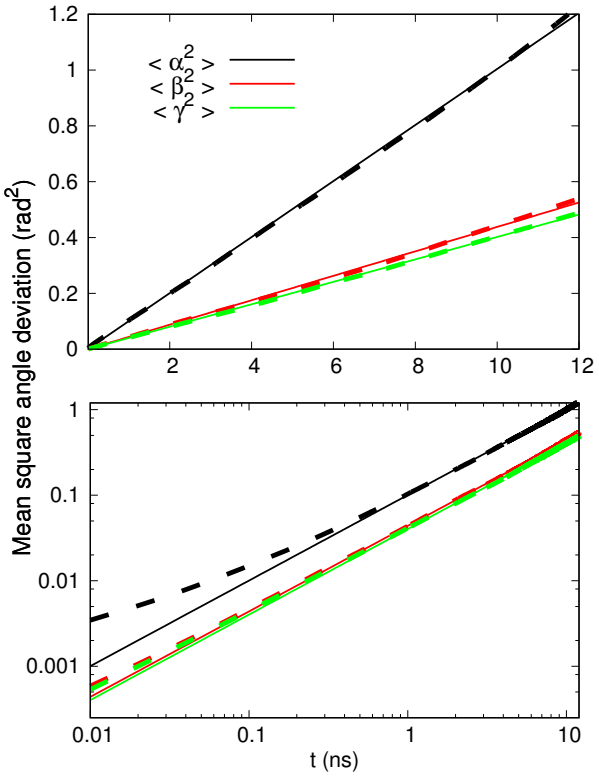

Figure 1: Mean square angle deviations of inertia tensor axes calculated from *Pa*TonB-96 simulation with OPC water model. The data shown with linear (top) and logarithmic scale (bottom).

The analysis leading to the new correlation functions in Eq. 13 (see Methods section) is exemplified in Fig. 2 for three residues locating in different domains of *Pa*TonB-96 with different characteristic rotational dynamics. The flexible C-terminus is represented by the residue 341, more rigid β-sheet by the residue 331 and a flexible loop between two β-strands by residue 322 (see the labeling in Fig. 6). The total correlation functions $C(t)$ of all the residues in Fig. 2 (top, solid lines) decay toward zero within ∼10-50 ns. The internal correlation functions $C_I(t)$ in Fig. 2 (middle) decay to a plateau value, which defines the square of the order parameter S^2. As expected, the internal correlation function for residue 331 in the rigid β-sheet rapidly decays to the largest order parameter value, while the correlation functions of the residues in the loop and C-terminus decay slower to the smaller order parameter values due to the larger conformational ensemble sampled by these regions.

The overall rotational correlation functions, $C_O(t) = C(t)/C_I(t)$, are shown in Fig. 2

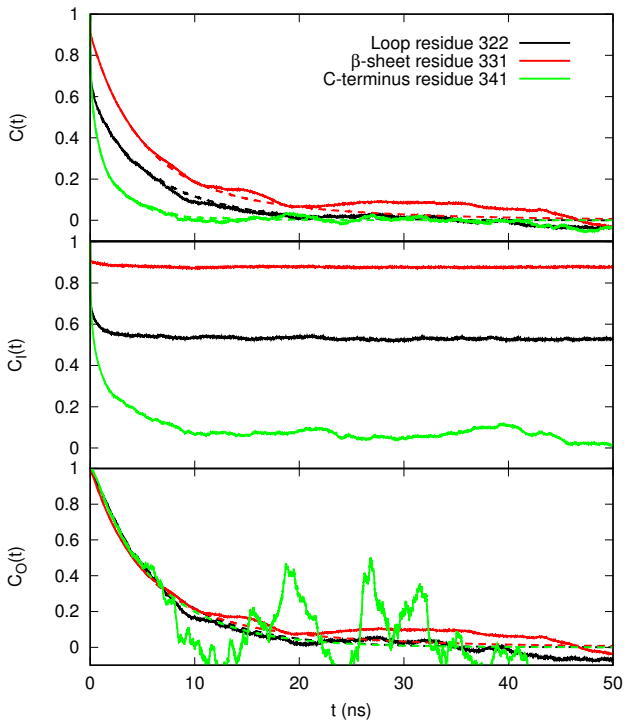

Figure 2: Rotational correlation functions calculated from MD simulations of *Pa*TonB-96 with tip4p water model at 298 K for residues at different regions. (top) total correlation functions $C(t)$ calculated from MD simulation (solid lines) and new correlation functions determined from Eqs. 6 and 8 by using rotational diffusion constants and fitted prefactors (dashed lines), (middle) correlation functions for internal motions calculated from simulation with removed overall protein rotation (bottom) correlation function for overall motions determined as $C_O(t) = C(t)/C_I(t)$ (solid lines) and by fitting to Eq. 8 with timescales from rotational diffusion coefficients in Table 1 (dashed lines).

(bottom, solid lines). Also the correlation functions of anisotropic rigid body rotation from Eq. 8 are shown in Fig. 2 (bottom, dashed lines). The timescales for the latter, τ_i, are given by the rotational diffusion coefficients from the simulation and the relations in Eq. 9. The prefactors, A_j, are determined by fitting Eq. 8 to the overall rotation correlation functions, $C_O(t)$, calculated from the MD simulation. The new correlation functions, determined from Eq. 13 and shown in Fig. 2 (top, dashed lines), are indistinguishable from the correlation functions calculated from the original MD simulations with the lag times shorter than one hundredth of total simulation time (approximately 4-12 ns), which is the maximum lag time for the good statistics in single molecule MD simulations.[27] This suggests that the anisotropic rigid body diffusion model (Eq. 8) and the separation of internal and global motions (Eq. 6)

are good approximations for the proteins studied in this work. The analytical description of the overall rotation with Eq. 8 in the new correlation functions clearly reduces the statistical fluctuations with the long lag times in Fig. 2. The effect is most visible for the flexible C-terminus (residue 341) having the smallest, thus the least detectable, contribution from the overall rotation of the protein due to the small order parameters .

Global rotational dynamics in simulations and experiments

Spin relaxation times of *Hp*TonB-92 are compared between the experiments and simulations using two different water models in Fig. 3. Simulations with tip3p water model differ from the experimental data and underestimate the T_1/T_2 ratio, suggesting too fast overall rotational diffusion dynamics.[63] This is in agreement with the previous study, where the overestimated rotational diffusion was attributed to the self-diffusion of tip3p.[25] On the other hand, simulation results with tip4p water model show better agreement with the experimental data in Fig. 3.

To see if the discrepancy in spin relaxation times for simulations with tip3p water model could be explained by the overestimated overall diffusion of the protein, the diffusion coefficients were divided by a constant factor of 2.9 before applying Eq. 13 to calculate the new correlation functions. The spin relaxation times calculated from the new correlation functions after scaling the rotational diffusion coefficients are, indeed, in good agreement with the experimental data in Fig. 4

Similar comparison for the spin relaxation times of *Pa*TonB-96 between experiments and simulations with tip4p and OPC4 water models is shown in Fig. 5. The experimentation of the OPC4 water model was inspired by the recent study reporting significant improvements in lipid monolayer simulations when this water model was used.[66] Since tip3p water model was observed to significantly overestimate the rotational diffusion of protein, it was not used in *Pa*TonB-96 simulations. The underestimation of T_1/T_2 ratio was also observed in the simulations of *Pa*TonB-96 with tip4p and OPC4 water models when compared with the

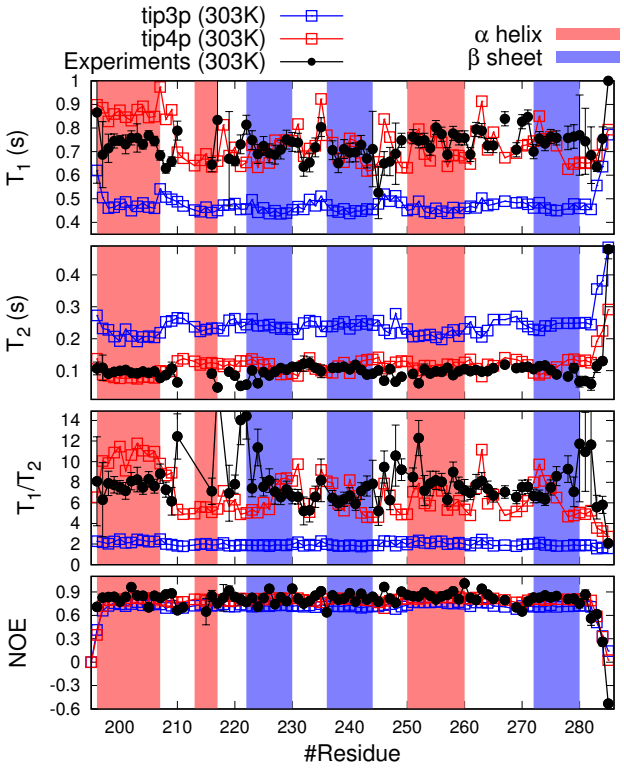

Figure 3: ^{15}N spin relaxation times for *Hp*TonB-92 from experimental data (circles) and MD simulations with different water models (squares).

experiments. The discrepancy is, however, less severe than for *Hp*TonB-92 simulated with tip3p in Fig. 3, suggesting that the required scaling factor for the overall rotational diffusion should be smaller for tip4p and OPC4 water models. Indeed, the spin relaxation times calculated from *Pa*TonB-96 simulation with tip4p water model were in good agreement with the experiments in Fig. 6 after the diffusion coefficients were divided with a constant factor of 1.2, which is smaller than 2.9 used for the *Hp*TonB-92 simulation above. Notably, the effect of 12 degree temperature difference on the spin relaxation times from tip4p simulations in Fig. 5 is significantly smaller than the observed differences between simulations and experiments or the changes due to the scaling of the diffusion coefficient.

The scaling of the overall rotational diffusion coefficients with a constant factor led to a good agreement with the experimental spin relaxation data for both systems simulated with different water models, as seen in Figs. 4 and 6. The good agreement with experiments suggests that the scaled rotational diffusion coefficients from MD simulations can be con-

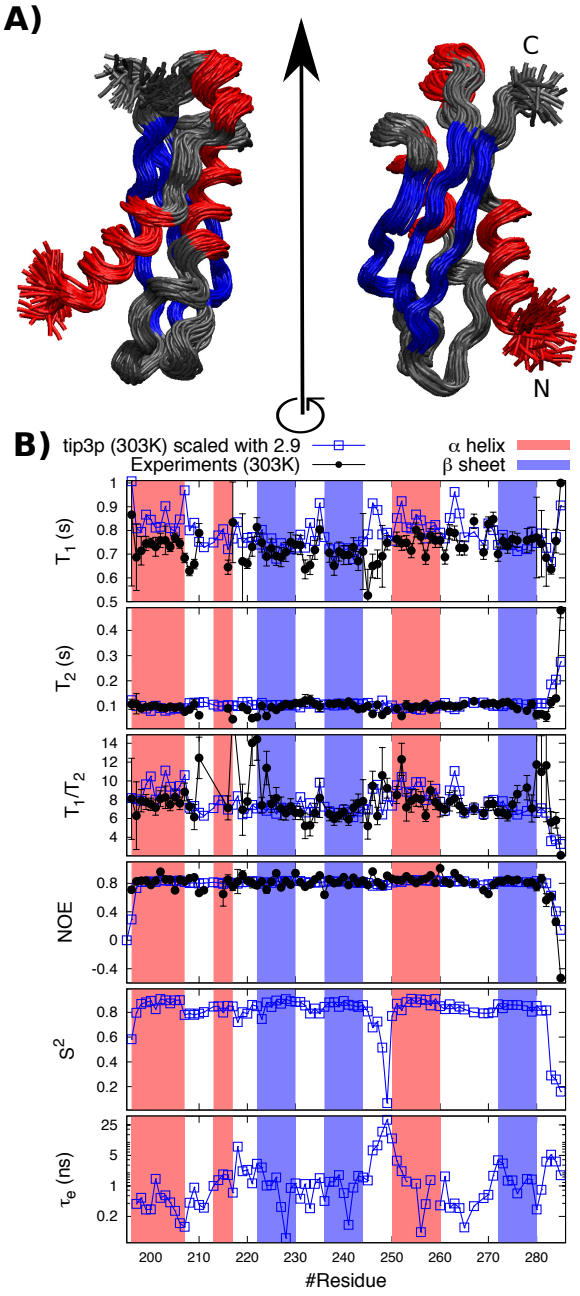

Figure 4: A) Structures of *Hp*TonB-92 from the MD simulations with tip3p at 303 K (100 structures taken from 400ns long trajectory). Secondary structures are color-labeled with Visual Molecular dynamics;[64,65] α-helices are red and β-strands are blue. Terminal ends are labelled with N and C. B) Spin relaxation times from experiments (circles) and tip3p simulations (squares) with rotational diffusion coefficients divided by a constant factor of 2.9 at 303 K. Order parameters and effective internal correlation times calculated from simulations

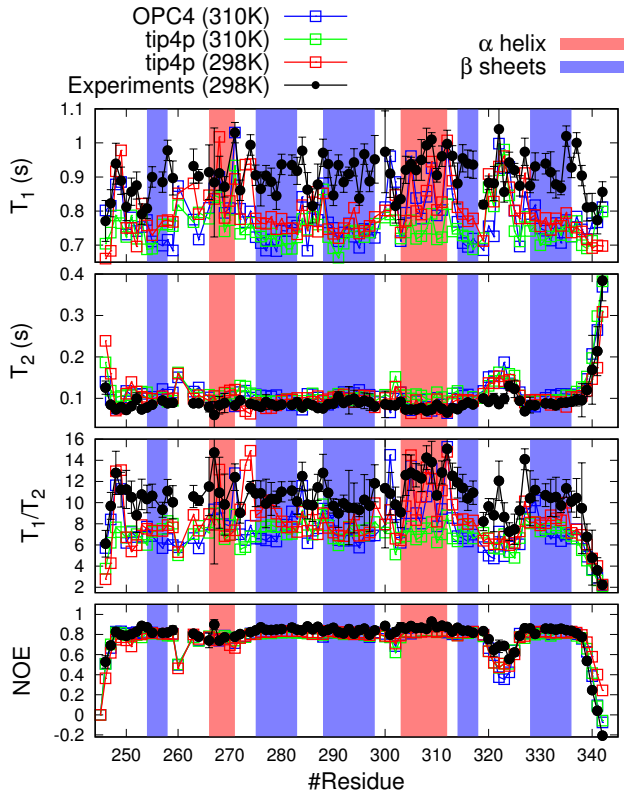

Figure 5: Plots of experimental (circles) and simulated (squares) spin relaxation times for *Pa*TonB-96.

sidered as a interpretation of the anisotropic rotational motion in NMR experiments. The scaled rotational diffusion coefficients from the simulations giving the best agreement with the experimental data are summarized in Table 2. In contrast to the unscaled diffusion constants in Table 1, these results are in line with the previously reported values for proteins with similar sizes.[62] Also the timescales, τ_c', estimated from Eq. 11 are close to the average diffusion coefficient, $\tau_c = (6D_{\mathrm{av}})^{-1}$, in Table 1.

Interpretation of protein internal relaxation from MD simulations

The good agreement of the spin relaxation times between the simulations with the scaled overall rotational diffusion coefficients and the experiments (Figs. 4 and 6) suggest that the simulations can be used to interpret the internal mobility of proteins from the experimental data.

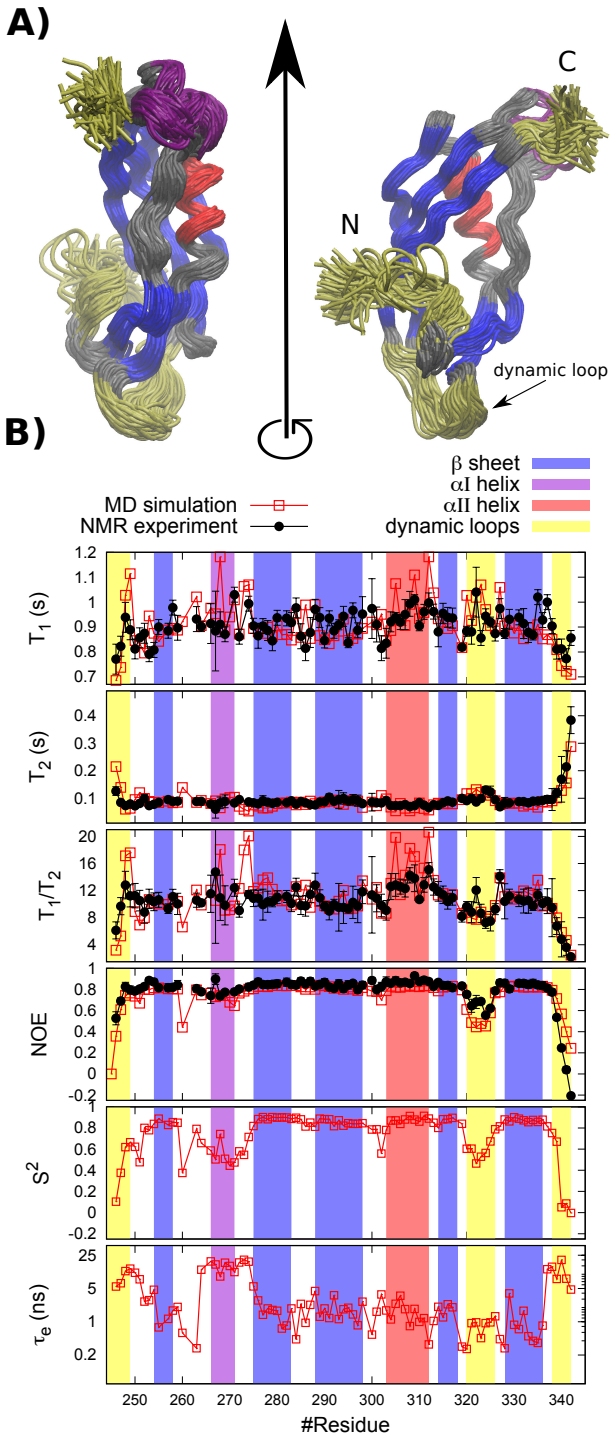

Figure 6: A) Structures sampled by *Pa*TonB-96 from MD simulations with tip4p at 298 K (100 structures from 400 ns long trajectory). Secondary structures are color labeled with Visual Molecular dynamics;[64,65] α-helixes and β-strands are red and blue, respectively. Residues 246-251, 320-326 and 338-342 with increased internal dynamics are yellow and α-helix fluctuations between two orientations (residues 266-270) is violet in the left column. Terminal ends are labelled with N and C. B) Spin relaxation times from experiments (circles) and tip4p simulations (squares) with rotational diffusion coefficients divided by a constant factor of 1.2 at 298 K. Order parameters and effective internal correlation times calculated from simulations.

Table 2: Rotational diffusion coefficients ($\mathrm{rad}^2 \cdot 10^7/\mathrm{s}$) giving the best agreement with experimental spin relaxation data. For *Hp*TonB-92 construct the values calculated from simulation with tip3p were scaled with 2.9 (spin relaxation data in Fig. 4) and for *Pa*TonB-96 the values from tip4p simulation at 298K were scaled by 1.2 (spin relaxation data in Fig. 6).

	*Hp*TonB-92	*Pa*TonB-96
D_x	2.15 ± 0.01	1.51 ± 0.01
D_y	2.43 ± 0.01	1.72 ± 0.03
D_z	4.10 ± 0.01	3.79 ± 0.03
D_{av}	2.90 ± 0.03	2.3 ± 0.02
$\tau_c(\mathrm{ns})^{\mathrm{a}}$	5.7 ± 0.1	7.2 ± 0.1
$\tau_c'(\mathrm{ns})^{\mathrm{b}}$	5.8 ± 0.1	6.9 ± 0.1

[a] $\tau_c = (6D_{\mathrm{av}})^{-1}$, [b] Average over all residues given by Eq. 11.

Only small variations between different residues are observed for spin relaxation times of *Hp*TonB-92 in Fig. 3. This indicates a rather rigid protein structure, which is also seen in the MD simulation snapshots overlayed in Fig. 3 A). Only few residues in the terminal ends show slightly enhanced conformational fluctuations in the MD simulation and in spin relaxation data. In addition, some deviations from the average spin relaxation times are observed in the experimental data close to residues 210-222. Simulations of *Hp*TonB-92 do not offer any explanation for this observation, however, the similar region in *Pa*TonB-96 simulation shows fluctuations between two orientations of α-helix.[29] Exceptionally low order parameters and long effective correlation times are observed in simulations for residues 245-250 of *Hp*TonB-92. Moreover, short T_1 times are experimentally observed close to this region, but the interpretation is not straightforward as the low T_1 times are not reproduced by MD simulations.

*Pa*TonB-96 exhibits more internal mobility and the segments with enhanced conformational fluctuations are labeled with yellow color in Fig. 6. Larger number of sampled conformations in both terminal ends are characterized by low order parameters and long effective internal correlation times observed in the simulations. Enhanced conformational fluctuations are also observed for residues 320-326, which correspond the loop between two β-strands.

MD simulations predict low order parameters and long internal effective correlation times also close to residues 266-271, which can be explained by two different orientations sampled by the α-helix in this region (color labeled with violet in Fig. 6 A). The orientational fluctuations of the similar short helix could also explain the above mentioned deviations of spin relaxation times for residues 210-222 of *Hp*TonB-92.[28]

MD simulations can be used to analyze different components contributing to the rotational dynamics of individual N-H bonds. In this work we have fitted a sum of 471 different timescales to the correlation functions according to Eq. 14. Most of the prefactors (α_i in Eq. 14) are zero in all the correlation functions after the fitting, thus the timescales τ_i corresponding non-zero prefactors are considered as the components contributing to the total relaxation process of each N-H bond. The prefactors are shown in Fig. 7 for the same residues of *Pa*TonB-96, which were used to exemplify the correlation functions in Fig. 2. As expected for residue 322 in the rigid β-sheet with large order parameter, the rotational relaxation is dominated by timescales of $\sim$5.5 ns and $\sim$8 ns, matching with the protein overall rotation. Also the dynamics of residue 322 in the flexible loop of *Pa*TonB is dominated by the timescales around $\sim$8 ns corresponding to the protein overall rotation, however, the fast motions from internal mobility are more evident than for the rigid β-sheet residue. This is in agreement with smaller order parameter observed in the flexible loop residues. On the other hand, the rotational dynamics of residue 341 in the flexible N-terminus of *Pa*TonB is dominated by timescales below 3 ns, most likely related to the internal motion of the protein. Contributions from timescales around $\sim$13 ns to the dynamics of residue 341 probably arise from the slow conformational fluctuations of the N-terminus, rather than the overall rotational dynamics. This supports the conclusion that the large amount of sampled conformations lead to the small order parameters and large effective correlation times observed in Fig. 5. While the separation of rotational dynamics of individual N-H bonds to different components gives intuitively understandable results, it should be kept in mind that it is based on the fitting of a multiexponential sum to the simulation data and the solution of

such fit is not unique.

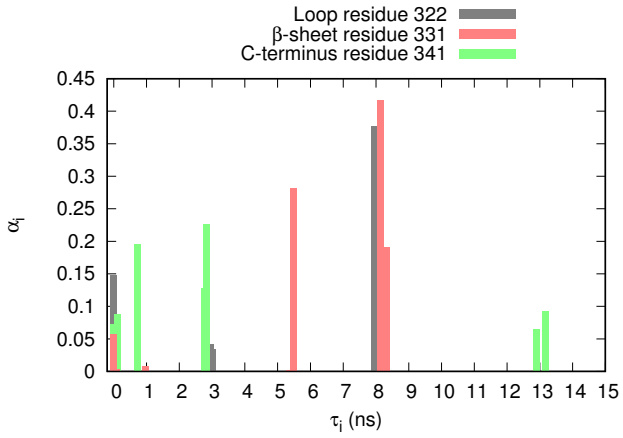

Figure 7: Prefactors α_i corresponding different timescales τ_i resulting from a fit of Eq.14 to correlation functions from MD simulation of *Pa*TonB-96 at 298K. The used correlation functions give a good agreement with experimental spin relaxation times as shown in Fig. 6.

Conclusions

The experimental spin relaxation data for protein backbone N-H bonds was successfully reproduced by using the classical molecular dynamics simulations for two different small domains. Thus, the simulation trajectories give an atomic resolution interpretation for protein dynamics measured with NMR experiments. Interpretation of the overall and internal dynamics was demonstrated for two proteins with anisotropic molecular shape and some flexible regions. Interpretation of the ^{15}N spin relaxation data measured from such proteins has been very challenging with the previously available methods.[22,61]

The overall rotation of the studied proteins was found to be brownian having only a small subdiffusive behavior with short timescales below ∼0.12 ns, which could be contrasted with crowded environments, where anomalous diffusion is expected to be more significant.[67] The direct analysis of classical molecular dynamics trajectories did not, however, reproduce the experimental ^{15}N spin relaxation data. Comparison between the rotational diffusion

coefficients and spin relaxation times between simulations and experiments suggested that the overall brownian tumbling of proteins is too rapid in the simulations, in agreement with the previous report suggesting that the discrepancy arises from the inaccuracies in water models.[25] Scaling down the anisotropic diffusion coefficients in the simulation data led to a good agreement with the experimental data.

Overall rotational diffusion coefficients were overestimated by a factor of ∼3 in the *Hp*TonB-92 simulations with tip3p water model, in line with previous studies.[24–26] Simulations with tip4p and OPC4 water models gave the spin relaxation times in reasonable agreement with experiments with scaling factors of ∼1-1.2, which is significantly less than for tip3p. It should be noted, however, that the correct scaling factors for the two different proteins, *Hp*TonB-92 and *Pa*TonB-96, simulated with the same water model, tip4p, seems to be 1 and 1.2, respectively. This suggests that the correction factor is not fully determined by the bulk water properties and that the hydration layer and water-protein interactions may play a critical role in rotational dynamics of proteins, as also suggested by the hydrodynamical calculations.[35]

Similarity between the correlation functions from the original MD trajectory and the new correlation functions from Eq. 13 suggest that the usage of the inertia axes and the separation of internal and the overall rotational motions (Eq. 6) are good approximations for the above investigated proteins. This is in line with the previous studies of other proteins with well defined structure.[10,25] However, it remains to be seen how well this and other related approaches[24,26] will succeed for intrinsically disordered proteins without the well defined shape. Since the correction of the incorrect overall rotational diffusion due to water model may become highly complicated for such proteins, it may be necessary to employ a water model giving correct overall rotational diffusion coefficients for biomolecules.

As further demonstrated in Ref. 29, the approach presented in this work can be used to interpret the rotational dynamics of proteins with anisotropic shape from ^{15}N spin relaxation data measured only with one magnetic field strength. This is a significant advancement

over currently available methods, which may not be applicable in such cases, even thought experimental data would be measured with multiple magnetic field strengths.

Acknowledgement

Academy of Finland (277335) and Sigrid Jusélius Foundation are acknowledged for the financial support to complete this work. The Finnish Biological NMR Center is supported by Biocenter Finland and HiLIFE-INFRA. We acknowledge CSC-IT center for science for computational resources.

Supporting Information Available

- Mean square angle deviations of *Pa*TonB-96 simulations with tip4p water at 310 K and 298 K

This material is available free of charge via the Internet at `http://pubs.acs.org/`.

References

(1) Jarymowycz, V. A.; Stone, M. J. Fast Time Scale Dynamics of Protein Backbones: NMR Relaxation Methods, Applications, and Functional Consequences. *Chem. Rev.* **2006**, *106*, 1624–1671.

(2) Korzhnev, D.; Billeter, M.; Arseniev, A.; Orekhov, V. NMR studies of Brownian tumbling and internal motions in proteins. *Prog. Nuc. Magn. Res. Spect.* **2001**, *38*, 197 – 266.

(3) Mulder, F. A.; Mittermaier, A.; Hon, B.; Dahlquist, F. W.; Kay, L. E. Studying excited states of proteins by NMR spectroscopy. *Nat. Struct. Mol. Biol.* **2001**, *8*, 932–935.

(4) Eisenmesser, E. Z.; Millet, O.; Labeikovsky, W.; Korzhnev, D. M.; Wolf-Watz, M.; Bosco, J. J., Daryl A. Skalicky; Kay, L. E.; Kern, D. Intrinsic dynamics of an enzyme underlies catalysis. *Nature* **2005**, *438*, 117–121.

(5) Van den Bedem, H.; Fraser, J. Dynamic Structural Biology at Atomic Resolution–It's About Time. *Nat. Methods* **2015**, *12*, 307–318.

(6) Lewandowski, J. R.; Halse, M. E.; Blackledge, M.; Emsley, L. Direct observation of hierarchical protein dynamics. *Science* **2015**, *348*, 578–581.

(7) Lamley, J. M.; Lougher, M. J.; Sass, H. J.; Rogowski, M.; Grzesiek, S.; Lewandowski, J. R. Unraveling the complexity of protein backbone dynamics with combined ^{13}C and ^{15}N solid-state NMR relaxation measurements. *Phys. Chem. Chem. Phys.* **2015**, *17*, 21997–22008.

(8) Yang, D.; Kay, L. E. Contributions to Conformational Entropy Arising from Bond Vector Fluctuations Measured from NMR-Derived Order Parameters: Application to Protein Folding. *J. Mol. Biol.* **1996**, *263*, 369 – 382.

(9) Kasinath, V.; Sharp, K. A.; Wand, A. J. Microscopic Insights into the NMR Relaxation-Based Protein Conformational Entropy Meter. *J. Am. Chem. Soc.* **2013**, *135*, 15092–15100.

(10) Allnér, O.; Foloppe, N.; Nilsson, L. Motions and Entropies in Proteins as Seen in NMR Relaxation Experiments and Molecular Dynamics Simulations. *J. Phys. Chem. B* **2015**, *119*, 1114–1128.

(11) Akke, M.; Brüschweiler, R.; Palmer, A. G. NMR order parameters and free energy: an analytical approach and its application to cooperative calcium(2+) binding by calbindin D9k. *J. Am. Chem. Soc.* **1993**, *115*, 9832–9833.

(12) Sanchez-Medina, C.; Sekhar, A.; Vallurupalli, P.; Cerminara, M.; Muñoz, V.; Kay, L. E. Probing the Free Energy Landscape of the Fast-Folding gpW Protein by Relaxation Dispersion NMR. *J. Am. Chem. Soc.* **2014**, *136*, 7444–7451.

(13) Best, R. B.; Vendruscolo, M. Determination of Protein Structures Consistent with NMR Order Parameters. *J. Am. Chem. Soc.* **2004**, *126*, 8090–8091.

(14) Showalter, S. A.; Brüschweiler, R. Validation of Molecular Dynamics Simulations of Biomolecules Using NMR Spin Relaxation as Benchmarks: Application to the AMBER99SB Force Field. *J. Chem. Theory Comput.* **2007**, *3*, 961–975.

(15) Showalter, S. A.; Johnson, E.; Rance, M.; Brüschweiler, R. Toward Quantitative Interpretation of Methyl Side-Chain Dynamics from NMR by Molecular Dynamics Simulations. *J. Am. Chem. Soc.* **2007**, *129*, 14146–14147.

(16) Maragakis, P.; Lindorff-Larsen, K.; Eastwood, M. P.; Dror, R. O.; Klepeis, J. L.; Arkin, I. T.; Jensen, M. Ø.; Xu, H.; Trbovic, N.; Friesner, R. A. et al. Microsecond Molecular Dynamics Simulation Shows Effect of Slow Loop Dynamics on Backbone Amide Order Parameters of Proteins. *J. Phys. Chem. B* **2008**, *112*, 6155–6158.

(17) Trbovic, N.; Kim, B.; Friesner, R. A.; Palmer, A. G. Structural analysis of protein dynamics by MD simulations and NMR spin-relaxation. *Proteins: Struct., Funct., Bioinf.* **2008**, *71*, 684–694.

(18) Wennerström, H.; Lindman, B.; Söderman, O.; Drakenberg, T.; Rosenholm, J. B. Carbon-13 magnetic relaxation in micellar solutions. Influence of aggregate motion on T1. *J. Am. Chem. Soc.* **1979**, *101*, 6860–6864.

(19) Lipari, G.; Szabo, A. Model-Free Approach to the interpretation of Nuclear Magnetic Resonance Relaxation in Macromolecules. 1. Theory and Range of Validity. *J. Am. Chem. Soc.* **1982**, *104*, 4546–4559.

(20) Woessner, D. E. Nuclear Spin Relaxation in Ellipsoids Undergoing Rotational Brownian Motion. *J. Chem. Phys.* **1962**, *37*, 647–654.

(21) Shimizu, H. Effect of Molecular Shape on Nuclear Magnetic Relaxation. *J. Chem. Phys.* **1962**, *37*, 765–778.

(22) Luginbühl, P.; Pervushin, K. V.; Iwaï, H.; Wüthrich, K. Anisotropic Molecular Rotational Diffusion in 15N Spin Relaxation Studies of Protein Mobility. *Biochemistry* **1997**, *36*, 7305–7312.

(23) Blake-Hall, J.; Walker, O.; Fushman, D. In *Protein NMR Techniques*; Downing, A. K., Ed.; Humana Press: Totowa, NJ, 2004; pp 139–159.

(24) Prompers, J. J.; Brüschweiler, R. General Framework for Studying the Dynamics of Folded and Nonfolded Proteins by NMR Relaxation Spectroscopy and MD Simulation. *J. Am. Chem. Soc.* **2002**, *124*, 4522–4534.

(25) Wong, V.; Case, D. A. Evaluating Rotational Diffusion from Protein MD Simulations. *J. Phys. Chem. B* **2008**, *112*, 6013–6024.

(26) Anderson, J. S.; LeMaster, D. M. Rotational velocity rescaling of molecular dynamics trajectories for direct prediction of protein NMR relaxation. *Biophys. Chem.* **2012**, *168*, 28 – 39.

(27) Lu, C.-Y.; Bout, D. A. V. Effect of finite trajectory length on the correlation function analysis of single molecule data. *J. Chem. Phys.* **2006**, *125*, 124701.

(28) Ciragan, A.; Aranko, A. S.; Tascon, I.; Iwaï, H. Salt-inducible Protein Splicing in cis and trans by Inteins from Extremely Halophilic Archaea as a Novel Protein-Engineering Tool. *J. Mol. Biol.* **2016**, *428*, 4573 – 4588.

(29) Oeemig, J. S.; Ollila, O. H. S.; Heikkinen, H. A.; Iwaï, H. The NMR structure of the C-terminal domain of TonB protein from *Pseudomonas aeruginosa*. **2018**, In preparation.

(30) Abragam, A. *The Principles of Nuclear Magnetism*; Oxford University Press, 1961.

(31) Kay, L. E.; Torchia, D. A.; Bax, A. Backbone dynamics of proteins as studied by nitrogen-15 inverse detected heteronuclear NMR spectroscopy: application to staphylococcal nuclease. *Biochemistry* **1989**, *28*, 8972–8979.

(32) Hiyama, Y.; Niu, C. H.; Silverton, J. V.; Bavoso, A.; Torchia, D. A. Determination of 15N chemical shift tensor via 15N-2H dipolar coupling in Boc-glycylglycyl[15N glycine]benzyl ester. *J. Am. Chem. Soc.* **1988**, *110*, 2378–2383.

(33) Halle, B. The physical basis of model-free analysis of NMR relaxation data from proteins and complex fluids. *J. Chem. Phys.* **2009**, *131*, 224507.

(34) Dosset, P.; Hus, J.-C.; Blackledge, M.; Marion, D. Efficient analysis of macromolecular rotational diffusion from heteronuclear relaxation data. *J. Biomol. NMR* **2000**, *16*, 23–28.

(35) de la Torre, J. G.; Huertas, M.; Carrasco, B. HYDRONMR: Prediction of NMR Relaxation of Globular Proteins from Atomic-Level Structures and Hydrodynamic Calculations. *J. Magn. Res.* **2000**, *147*, 138 – 146.

(36) Fisette, O.; Lagüe, P.; Gagné, S.; Morin, S. Synergistic Applications of MD and NMR for the Study of Biological Systems. *J. Biomed. Biotechnol.* **2012**, *2012*, 254208.

(37) Gu, Y.; Li, D.-W.; Brüschweiler, R. NMR Order Parameter Determination from Long Molecular Dynamics Trajectories for Objective Comparison with Experiment. *J. Chem. Theory Comput.* **2014**, *10*, 2599–2607.

(38) 2017; DOI: 10.5281/zenodo.1010416.

(39) 2017; DOI: 10.5281/zenodo.1010406.

(40) 2017; DOI: 10.5281/zenodo.1010438.

(41) 2017; DOI: 10.5281/zenodo.1010232.

(42) 2017; DOI: 10.5281/zenodo.1010142.

(43) 2017; DOI: 10.5281/zenodo.1010238.

(44) 2017; DOI: 10.5281/zenodo.1010352.

(45) 2017; DOI: 10.5281/zenodo.1010357.

(46) Abraham, M. J.; Murtola, T.; Schulz, R.; Páll, S.; Smith, J. C.; Hess, B.; Lindahl, E. GROMACS: High performance molecular simulations through multi-level parallelism from laptops to supercomputers. *SoftwareX* **2015**, *1-2*, 19 – 25.

(47) Lindorff-Larsen, K.; Piana, S.; Palmo, K.; Maragakis, P.; Klepeis, J. L.; Dror, R. O.; Shaw, D. E. Improved side-chain torsion potentials for the Amber ff99SB protein force field. *Proteins: Struct., Funct., Bioinf.* **2010**, *78*, 1950–1958.

(48) Jorgensen, W. L.; Chandrasekhar, J.; Madura, J. D.; Impey, R. W.; Klein, M. L. Comparison of simple potential functions for simulating liquid water. *J. Chem. Phys.* **1983**, *79*, 926–935.

(49) Izadi, S.; Anandakrishnan, R.; Onufriev, A. V. Building Water Models: A Different Approach. *J. Phys. Chem. Lett.* **2014**, *5*, 3863–3871.

(50) Bussi, G.; Donadio, D.; Parrinello, M. Canonical sampling through velocity rescaling. *J. Chem. Phys.* **2007**, *126*.

(51) Parrinello, M.; Rahman, A. Polymorphic transitions in single crystals: A new molecular dynamics method. *J. Appl. Phys.* **1981**, *52*, 7182–7190.

(52) Darden, T.; York, D.; Pedersen, L. Particle mesh Ewald: An N·log(N) method for Ewald sums in large systems. *J. Chem. Phys.* **1993**, *98*, 10089–10092.

(53) Essman, U. L.; Perera, M. L.; Berkowitz, M. L.; Larden, T.; Lee, H.; Pedersen, L. G. A smooth particle mesh ewald potential. *J. Chem. Phys.* **1995**, *103*, 8577–8592.

(54) Hess, B. P-LINCS: A Parallel Linear Constraint Solver for Molecular Simulation. *J. Chem. Theory Comput.* **2008**, *4*, 116–122.

(55) Abraham, M.; van der Spoel, D.; Lindahl, E.; Hess, B.; the GROMACS development team, GROMACS user manual version 5.0.7. 2015.

(56) McGibbon, R. T.; Beauchamp, K. A.; Harrigan, M. P.; Klein, C.; Swails, J. M.; Hernández, C. X.; Schwantes, C. R.; Wang, L.-P.; Lane, T. J.; Pande, V. S. MDTraj: A Modern Open Library for the Analysis of Molecular Dynamics Trajectories. *Biophys. J.* **2015**, *109*, 1528 – 1532.

(57) MATLAB, R2016a, The MathWorks, Inc., Natick, Massachusetts, United States.

(58) Nowacka, A.; Bongartz, N.; Ollila, O.; Nylander, T.; Topgaard, D. Signal intensities in ^{1}H–^{13}C CP and INEPT MAS NMR of liquid crystals. *J. Magn. Res.* **2013**, *230*, 165 – 175.

(59) Ferreira, T. M.; Ollila, O. H. S.; Pigliapochi, R.; Dabkowska, A. P.; Topgaard, D. Model-free estimation of the effective correlation time for C-H bond reorientation in amphiphilic bilayers: ^{1}H-^{13}C solid-state NMR and MD simulations. *J. Chem. Phys.* **2015**, *142*, 044905.

(60) 2017; https://github.com/ohsOllila/ProteinDynamics.

(61) Barbato, G.; Ikura, M.; Kay, L. E.; Pastor, R. W.; Bax, A. Backbone dynamics of calmodulin studied by nitrogen-15 relaxation using inverse detected two-dimensional NMR spectroscopy: the central helix is flexible. *Biochemistry* **1992**, *31*, 5269–5278.

(62) Krishnan, V.; Cosman, M. An empirical relationship between rotational correlation time and solvent accessible surface area. *J. Biomol. NMR* **1998**, *12*, 177–182.

(63) Carper, W. R.; Keller, C. E. Direct Determination of NMR Correlation Times from Spin-Lattice and Spin-Spin Relaxation Times. *J. Phys. Chem. A* **1997**, *101*, 3246–3250.

(64) Frishman, D.; Argos, P. Knowledge-based protein secondary structure assignment. *Proteins: Struct., Funct., Bioinf.* **1995**, *23*, 566–579.

(65) Humphrey, W.; Dalke, A.; Schulten, K. VMD – Visual Molecular Dynamics. *J. Mol. Graph.* **1996**, *14*, 33–38.

(66) Javanainen, M.; Lamberg, A.; Cwiklik, L.; Vattulainen, I.; Ollila, O. S. Atomistic Model for Near-Quantitative Simulations of Langmuir Monolayers. 2017; `http://dx.doi.org/10.1021/acs.langmuir.7b02855`.

(67) Höfling, F.; Franosch, T. Anomalous transport in the crowded world of biological cells. *Rep. Prog. Phys.* **2013**, *76*, 046602.

Graphical TOC Entry